Applied Catalysis B: Environmental 123–124 (2012) 221–228

Contents lists available at SciVerse ScienceDirect

Applied Catalysis B: Environmental

journal homepage: www.elsevier.com/locate/apcatb

Structured fibrous carbon-based catalysts for continuous nitrate removal from natural water

T. Yuranova[a], C. Franch[b], A.E. Palomares[b], E. Garcia-Bordejé[c], L. Kiwi-Minsker[a,*]

[a] Ecole Polytechnique Fédérale de Lausanne, GGRC-EPFL, Lausanne, CH-1015, Switzerland
[b] Instituto de Tecnología Química, UPV-CSIC, Universidad Politécnica de Valencia, Camino Vera s.n., Valencia, 46022, Spain
[c] Instituto de Carboquimica, ICB-CSIC, Miguel Luesma Castan 4, Zaragoza, 50018, Spain

ARTICLE INFO

Article history:
Received 22 December 2011
Received in revised form 6 March 2012
Accepted 4 April 2012
Available online 2 May 2012

Keywords:
Nitrate removal
Structured fibrous carbon-based catalysts
Bimetallic
Nanofibers
Nanoparticles

ABSTRACT

Bimetallic (Pd–Cu, Pd–Sn) nanoparticles supported on structured fibrous carbons (activated carbon fibers and carbon nanofibers grown on sintered metal fibers) were tested in nitrate removal of natural polluted water by hydrogen (a batch and continuous mode). Dependence of the activity/selectivity on catalyst chemical composition, promoter nature and metal particle size was studied. Sn-modified Pd nanoparticles showed higher N_2 selectivity as compared to Cu-modified ones. The structured (Pd–Sn) nanoparticles supported on carbon nanofibers grown on Inconel sintered metal fibers demonstrated the best catalytic performance in an open flow reactor, providing optimal hydrodynamics properties.

1. Introduction

Catalytic reduction of nitrates to N_2 is one of the most promising, environmentally benign methods of their removal from polluted natural water [1–6]. Many efforts have been made to find selective catalysts for this process, since the formation of by-products, such as nitrites and ammonia sacrifices the initial idea. Supported Pd^0-nanoparticles modified by a second metal (Cu, Sn) have been found the most effective [7–15]. However, these catalysts are still quite sensitive to the chemical composition of treated water and to the operation conditions [16–19].

Reactant and/or product diffusion limitations in the catalyst pores lead to a decrease of the selectivity to nitrogen. Moreover, technical applications of conventional powdered catalysts face also difficulties associated with either a high pressure drop and flow maldistribution in a fixed bed (continuous mode) or with an additional step of catalyst filtration (batch mode).

Structured catalysts such as monoliths, foams and grids eliminate such problems [20,21]. Structured fibrous supports (woven glass, carbon and sintered metal fibers (SMF)) composed of micron sized elementary filaments allow combining a high surface area and decreased internal diffusion limitations with surface properties [22–24].

Carbon has advantages over oxide support materials in aqueous phase processes [25–28] due to stability in acidic and alkaline media. At the same time, carbon surface chemistry is easily tuned through different treatments. Thus, surface hydrophilicity/hydrophobicity and adsorption properties can be controlled.

Pd–Cu supported on woven activated carbon fibers (ACF) has been already used for catalytic nitrate hydrogenation in both continuous and batch modes and demonstrated promising result (~90% selectivity towards N_2) when using distilled water containing nitrates [29]. The main drawback of ACF-based catalysts is that their microporosity and diffusion limitations in an aqueous phase can affect reaction selectivity.

Carbon nanofibers (CNF) represent a new type of carbon-based supports [30]. They share with activated carbons many common properties such as chemical inertness, mechanical stability and good thermal conductivity. Contrary to activated carbons, CNF do not have microporosity that could be very favorable for liquid-phase processes to avoid internal diffusion limitations. However, conventional CNF are fine powders, unless they are grown as a film on a macrostructured support. There are several examples of structured CNF used as catalyst supports: CNF on sintered metal fibers (CNF/SMF) [31,32] and CNF on carbon felt [33].

The objective of this work is to study catalytic nitrate reduction in both semi-batch and open-flow reactors over bimetallic nanoparticles (Pd–Cu, Pd–Sn) supported on different structured carbon materials: microporous ACF and mesoporous CNF/SMF. A special attention is given to the catalyst selectivity towards N_2 since

* Corresponding author. Tel.: +41 0 21 693 31 82; fax: +41 0 21 693 60 91.
E-mail address: lioubov.kiwi-minsker@epfl.ch (L. Kiwi-Minsker).

0926-3373/$ – see front matter © 2012 Elsevier B.V. All rights reserved.
http://dx.doi.org/10.1016/j.apcatb.2012.04.007

this is the key issue for environmental applications. Both natural and distilled waters containing NO_3^- were used because the activity and selectivity of the catalyst is very different depending on the type of water [26].

2. Experimental

2.1. Materials

Palladium (II) chloride anhydrous ($PdCl_2$, p.a.), palladium (II) acetate ($Pd(CH_3COO)_2$, p.a.), tin (II) chloride anhydrous ($SnCl_2$, p.a.), and sodium chloride (NaCl, p.a.) were purchased from Fluka (Buchs, Switzerland). The Na_2PdCl_4 was prepared by dissolving equivalent amounts of $PdCl_2$ and NaCl in water. The copper (II) formate ($Cu(HCOO)_2$, p.a.) was purchased from Aldrich (Buchs, Switzerland). Deionized water was used throughout the study. All gases (>99.99%) were purchased from Carbagas (Switzerland) and used as received.

Activated carbon fibers in the form of woven fabrics (AW1101, KoTHmex, Taiwan Carbon Technology Co.) were used as a catalyst support. Before metal deposition ACF were boiled in 15% HNO_3 for 1 h, then rinsed with water and dried in air. SSA_{BET} of the acid treated ACF (measured by N_2 adsorption–desorption at −196 °C *via* a Sorptomatic 1990) was ~950 $m^2\ g^{-1}$.

Commercially available Inconel sintered metal fibers (SMF), (Inconel 601, Bekipor ST20AL3, thickness – 0.49 mm, elementary fiber diameter – 8 μm, Bakaert Fiber Technology, Belgium) were used as a growth-media for carbon nanofibers. Chemical composition of the material is following: Ni – 60.5%; Cr – 23%; Al – 1.25%; Cu – 1%; Mn – 1%; Si – 0.5%; C – 0.1%; S – 0.015% and Fe – balance. Before use, SMF panels were calcined at 650 °C for 3 h in order to oxidize the fiber surface. The SMF panels were subsequently cut into round disks (d = 24 mm). The method of carbon nanofibers growing on SMF is described elsewhere [31]. Briefly, CNF were grown on SMF by the catalytic pyrolysis of ethane in the presence of hydrogen. The synthesis was carried out in a tubular quartz reactor with 24 mm internal diameter posed in a tubular oven. The SMF filters were first treated by hydrogen (625 °C, 2 h, 120 ml/min) in order to create Ni nanoparticles – catalyst of CNF growing – on the fiber surface. Then, the reactor was heated up 675 °C, and a mixture $Ar:C_2H_6:H_2$ = 80:3:17 (600 ml/min) was introduced for 2 h.

The obtained 5%CNF/SMF composite supports were activated in a boiling 30% H_2O_2 aqueous solution during 1 h. The samples were then treated ultrasonically in ethanol using a Bransonic ultrasonic cleaner (HF-output power nom. 30 W, Branson Ultrasonics Corp., USA) during 180 min. The weight loss after the H_2O_2 and ultrasonic treatments were not more than 0.5% of the initial weight of 5%CNF/SMF samples.

2.2. Catalyst preparation

2.2.1. ACF-based catalysts

The bimetallic (Pd–Cu)/ACF and (Pd–Sn)/ACF catalysts were prepared in two stages. First, Pd was deposited *via* adsorption of Na_2PdCl_4 from a diluted aqueous solution under stirring at room temperature (4 h). The amount of Na_2PdCl_4 in the solution was set to attain a desired loading of Pd^0 on ACF. After adsorption the material was rinsed with water, air-dried at room temperature and reduced by H_2 at 300 °C for 2 h.

On the second step of the (Pd–Cu)/ACF catalyst preparation, a certain amount of Pd^0/ACF was immersed into a solution of $Cu(HCOO)_2$ for 3 h. Catalytic electroless copper deposition ($Cu(HCOO)_2 = Cu^0 + CO_2 + HCOOH$) took place selectively on Pd^0 nanoparticles [29]. The concentration of $Cu(HCOO)_2$ solution was calculated in order to have the final Pd:Cu ratio equal 2. Then obtained material was rinsed with water, air-dried and treated in Ar for 2 h at 300 °C.

In the case of (Pd–Sn)/ACF catalysts, Pd/ACF was impregnated by a $SnCl_2$ ethanol solution of a certain concentration (in order to have the final Pd:Sn ratio equal to 2). After impregnation the material was air-dried at room temperature and treated in Ar at 300 °C for 2 h.

The metal loadings were confirmed by a chemical analysis using atomic absorption spectroscopy (AAS).

2.2.2. CNF/SMF-based catalysts

The bimetallic Pd–Cu and Pd–Sn catalysts based on activated 5%CNF/SMF were prepared in two stages. First, Pd was deposited on 5%CNF/SMF by incipient wetness impregnation using $Pd(CH_3COO)_2$ dissolved in acetonitrile as a precursor. After impregnation material was dried at room temperature and reduced by H_2 at 300 °C for 2 h. The concentration of the impregnation solution was set to have the final Pd^0 loading equal to 0.3 wt%.

On the second step of the (Pd–Cu)/5%CNF/SMF catalyst preparation, a $Cu(HCOO)_2$ solution of a calculated concentration (in order to have the final Pd:Cu ratio equal to 2) was impregnated into the reduced 0.3%Pd/5%CNF/SMF. Since Pd^0 is a catalyst of copper formate decomposition, Cu^0 is selectively deposited on Pd^0 nanoparticles. After treatment the samples were air-dried at room temperature and treated by Ar at 300 °C for 2 h.

In the case of (Pd–Sn)/5%CNF/SMF catalysts, a $SnCl_2$ ethanol solution of a certain concentration (in order to have the final Pd:Sn ratio equal to 2) was impregnated into the 0.3%Pd/5%CNF/SMF. After impregnation the samples were air-dried at room temperature and treated in Ar at 300 °C for 2 h.

2.3. Catalyst characterization

The metal loading (Pd, Cu, Sn) on the synthesized catalysts was measured through an atomic absorption spectroscopy (AAS) using a Shimadzu AA-6650 spectrophotometer with an air–acetylene flame. Prior to analysis the catalyst samples were dissolved in a mixture of nitric and hydrochloric acid (aqua regia). The ACF- and CNF/SMF-based catalysts before dissolving were calcined in air at 700 °C for 2 h in order to burn out the carbon.

The specific surface areas (SSA) of the carbon based composites were measured by adsorption–desorption of saturated nitrogen at −196 °C using a Sorptomatic 1990 instrument (Carlo Erba). The structured catalysts were cut into slices and placed in the reactor for measurement. The SSA was calculated employing the BET method. The Dollimore/Heal approach was applied to calculate the pore volume and size.

SEM analysis used to examine the morphology of the structured materials was carried out using a microscope SEM EDX Hitachi S-3400 N with variable pressure up to 270 Pa and an analyzer EDX Röntec XFlash de Si(Li). The images were obtained both from the secondary and backscattered signal.

For metal nanoparticles characterization scanning transmision electron microscopy (STEM) was carried out using a FEI-Tecnai F30 with a field emission gun working at 300 kV. The equipment magnification range operates between 150× and 230 M×. The preparation of the samples was carried out by scratching the material surface with a spatula, the retrieved powder was dispersed in ethanol by ultrasonication.

Local chemical composition was examined by X-ray energy-dispersive analysis (EDS).

2.4. Catalytic activity measurement

The catalysts were tested in both a discontinuous stirred tank reactor (semi-batch mode) and a flow–through fixed bed reactor

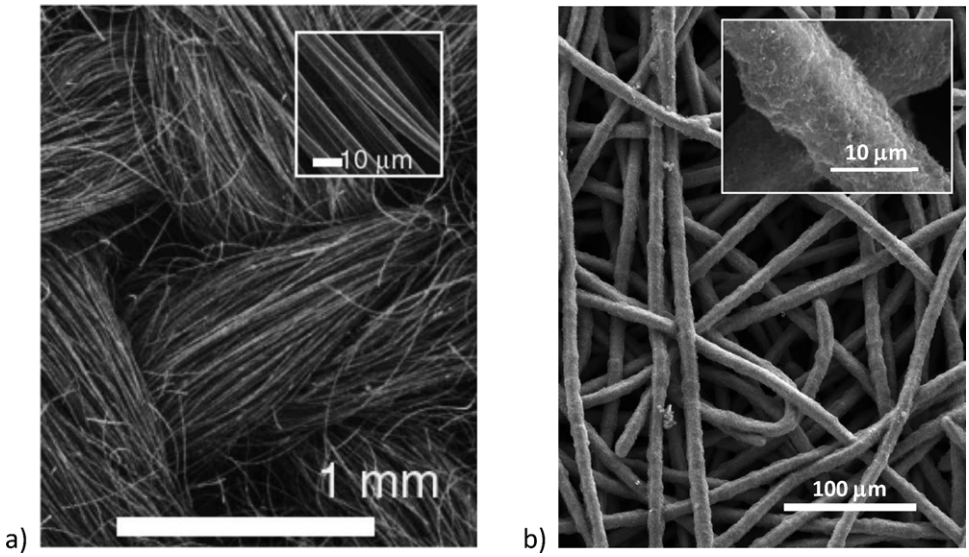

Fig. 1. Carbon-based structured supports: (a) ACF and (b) 5%CNF/SMF.

(continuous mode). The batch experiments were carried out in a 1-liter glass reactor equipped with a mechanical Teflon stirrer at room temperature and atmospheric pressure using distilled water containing 100 ppm of nitrates. Before reaction, the liquid solution (0.6 l) was bubbled with hydrogen during 1 h. The catalyst was cut into small particles and it was introduced into the reactor. The catalyst loading was in the range of 0.8–5 g/l. A gas flow with a H_2:CO_2 ratio of 1:1 was continuously passed through the solution using a glass frit (pH 6.5). The gas flow was 500 cm^3/min. The stirring rate was 900 rpm. The reaction progress was followed by withdrawing small aliquots for the photometric determination of nitrate, nitrite and ammonia concentration.

Catalytic reduction of nitrates in a flow–through fixed bed reactor was made using polluted natural water from an aquifer (Comunidad Valenciana, Spain). The main characteristics of this water are: pH 8; conductivity – 1000 μS/cm; COD – 2.3 mg/l; TOC – 70 mg/l; NO_3^- – 100 mg/l; SO_4^{2-} – 200 mg/l; Cl^- – 79 mg/l; Na^+ – 50 mg/l and Ca^{2+} – 150 mg/l.

The solution was pre-saturated with hydrogen before reaction. The reactant liquid was flown at 5 ml/min through the tubular reactor (inner diameter – 1.5 cm, length – 14.5 cm) together with 500 ml/min of a $CO_2 + H_2$ gas mixture (CO_2:H_2 = 1) (pH 6.5). The reaction was carried out at room temperature and atmospheric pressure.

In the continuous experiments with ACF-based catalysts, the catalyst loading was in the range of 1–3 g. In the continuous experiments with SMF-based catalysts, the diameter of the SMF filter exactly fitted to the reactor inner diameter operating as a conventional fixed bed reactor with the catalyst loading of 0.8–1.6 g. The reaction progress was followed by withdrawing small aliquots for the photometric determination of nitrate, nitrite and ammonia concentrations. The measurements were done with an UV–vis spectroscopy (Jasco UV–vis spectrophotometer, V-530) combined with reagent kits for the determination of nitrate (Spectroquant® nitrate test from Merck, measuring range 1 – 90 mg/l at 515 nm), nitrite (Spectroquant® nitrite test from Merck, measuring range 0.02 – 3 mg/l at 525 nm) and ammonia (Spectroquant® ammonia test from Merck, measuring range 0.01 – 3.5 mg/l at 690 nm).

The possible formation of N_2O was controlled by taking gaseous samples from the reactor and analyzing them by gas chromatography. No formation of N_2O was detected. The selectivity towards nitrite was calculated as $mol_{NO_2^-}/mol_{NO_3^-\,reduced}$. The selectivity towards ammonia was calculated as $mol_{NH_4^+}/mol_{NO_3^-\,reduced}$ and the selectivity to nitrogen was calculated by a difference.

Metal (Pd, Cu and Sn) concentrations were measured by Atomic Absorption Spectroscopy in treated waters after long-term runs. No metal leaching was detected. For the comparison of different catalysts, the catalyst activity defined as $mol_{NO_3^-\,reduced}/mol_{Pd} \cdot S$ together with the selectivity towards ammonia, nitrite and nitrogen were used.

3. Results and discussions

3.1. Structured carbon-based supports

Two carbon-based structured materials were used as supports for the bimetallic catalysts: an ACF fabric and carbon nanofibers grown on a sintered metal fiber (CNF/SMF) filter. The SEM images of the materials are presented in Fig. 1.

ACF fabric is woven from the threads of ~0.6 mm in diameter. These threads consist of a bundle of elementary filaments of ~5 μm in diameter. The oxidative treatment with nitric acid removes impurities and forms oxygen-containing groups [34]. The SSA of ACF after this treatment slightly increases from 880 to 950 m^2/g. The specific pore volume is equal to 0.58 cm^3/g. The ACF pore network is formed by short micropores with a narrow pore size distribution [35]. Most of them have a diameter <2 nm.

The specific surface area of SMF is negligible and just equal to a geometrical outer surface area of their constituent metal filaments (~0.5 m^2/g). Therefore, a thin porous layer of a catalyst support (*e.g.* carbon nanofibers (CNF)) should be created on the fiber surface. A high SSA of the support allows having a high dispersion of the deposited catalytically active phase. With increase of the CNF loading on SMF, SSA of CNF/SMF composites increases. At the same time, a too high CNF loading leads to the decrease of the empty space between metal fibers and to high pressure drops which is detrimental during reactor operation. It has been found that the 5–6 wt% CNF loading on SMF giving a SSA of ~15 m^2/g is an optimum for a high dispersed metal deposition avoiding high pressure drops [31]. Samples with the carbon content of ~5 wt% were used through this study. The average thickness of the CNF layer was measured by SEM to be ~1.5 μm. The diameter of an elementary carbon nanofiber is ~60 nm. The calculated SSA_{CNF} of the 5%CNF/SMF samples is ~260 m^2/g_{CNF}. The specific pore volume is equal to 0.62 cm^3/g_{CNF}. The CNF/SMF adsorption–desorption isotherms (Fig. 2) form a

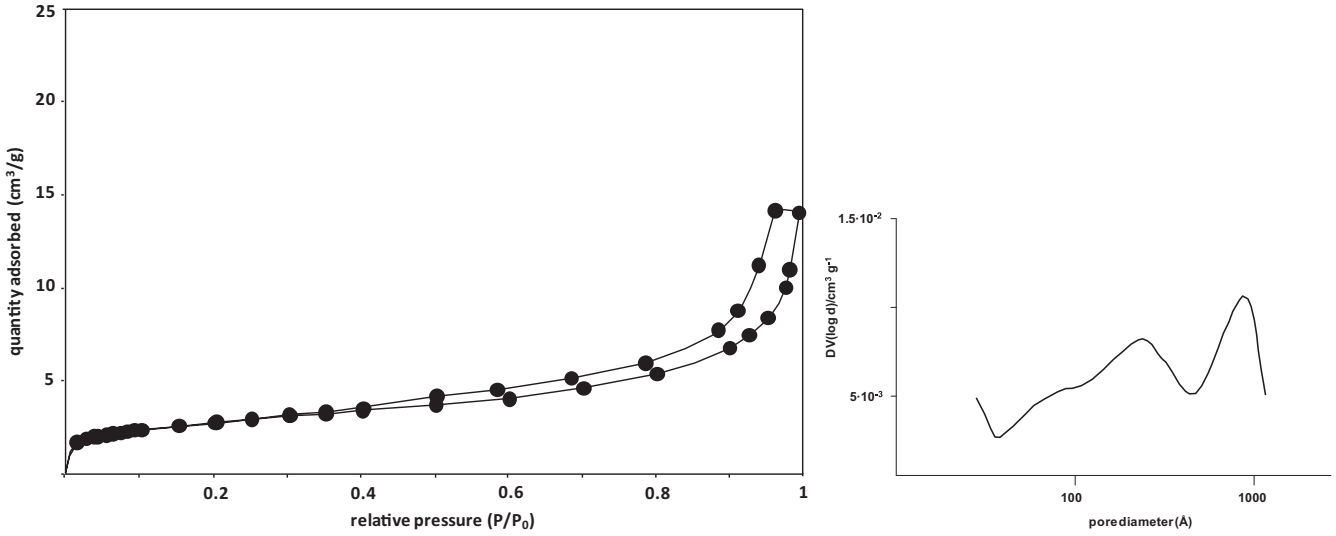

Fig. 2. Adsorption–desorption isotherms for the CNF/SMF and BHJ adsorption pore size distribution.

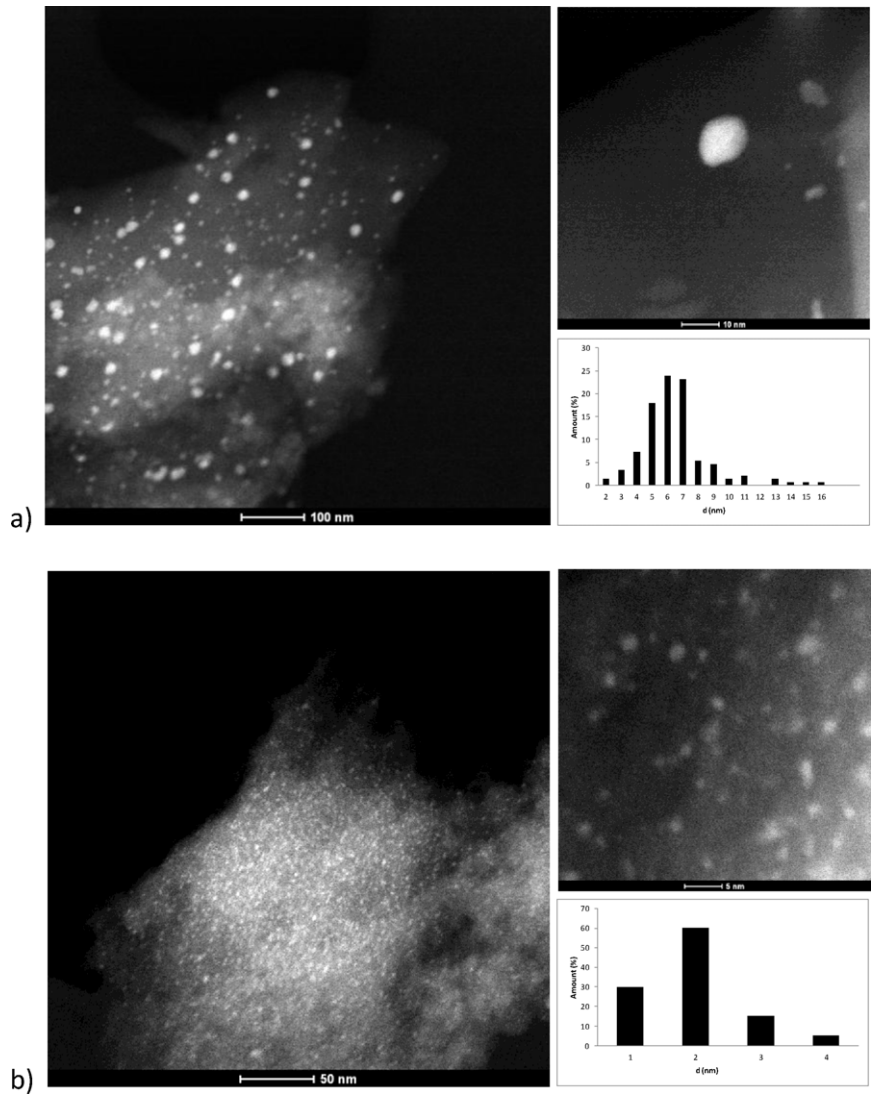

Fig. 3. STEM images of the ACF-based structured catalysts: (a) (5%Pd + 2.5%Cu)/ACF and (b) (2%Pd + 1%Sn)/ACF.

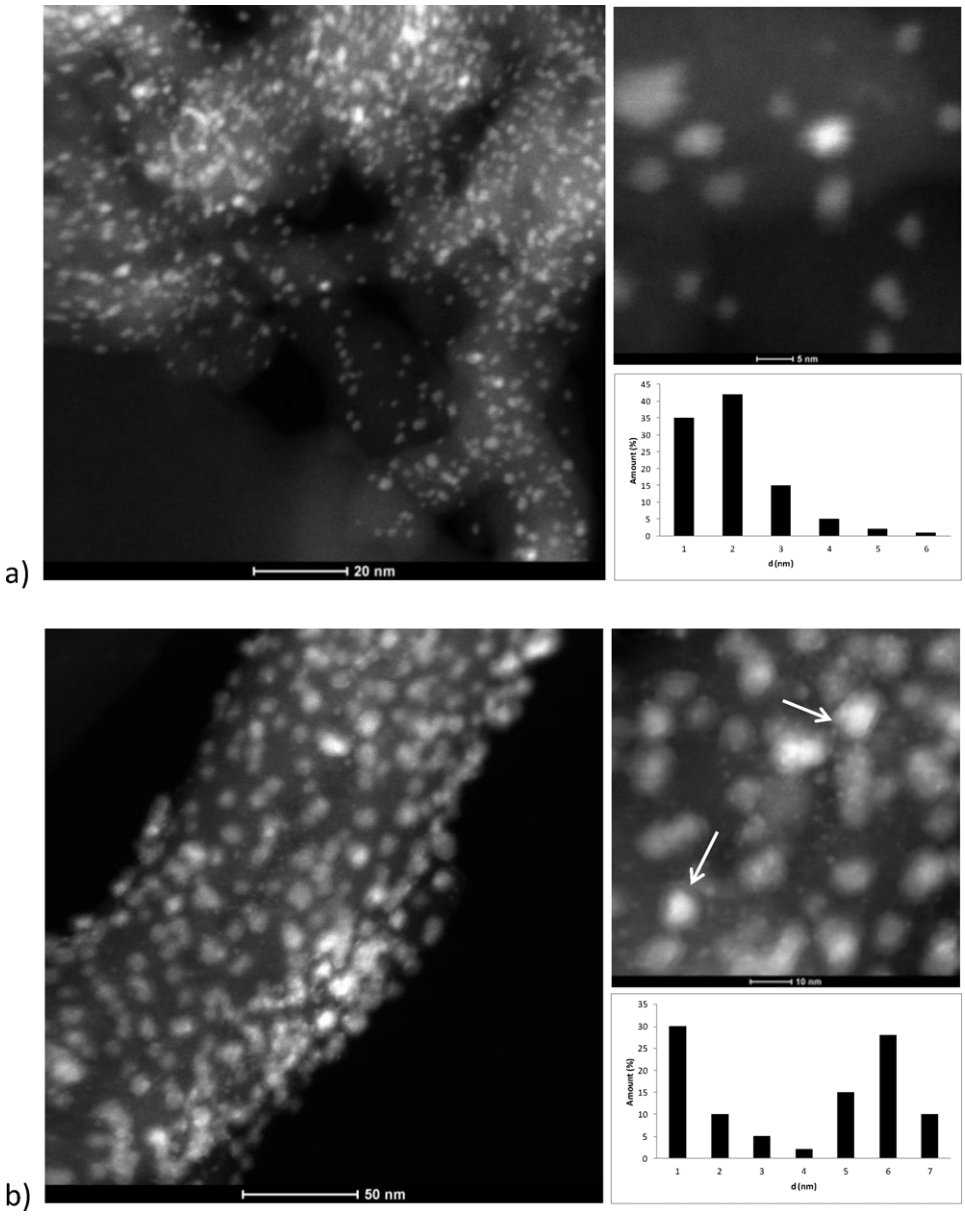

Fig. 4. STEM images of the CNF/SMF-based structured catalysts: (a) (0.3%Pd + 0.15%Cu)/5%CNF/SMF and (b) (0.3%Pd + 0.15%Sn)/5%CNF/SMF.

hysteresis loop with sharp adsorption and desorption branches at high relative pressures corresponding to type IV behavior and indicating that the material is mostly mesoporous. The pore size distribution is bimodal with peaks at 20 and 85 nm.

3.2. Bi-metallic structured carbon-based catalysts

All materials used in this study and some of their characteristics are listed in Table 1. The synthesized supported catalysts retain all textural properties of the carbon-based supports.

The representative STEM images of the bimetallic carbon-based catalysts are shown in Figs. 3 and 4. Due to the STEM technique, bimetallic nanoparticles are much more contrasted against the carbon support. Moreover, sometimes this technique allows discriminating between different metals, because the contrast is a function of the atomic number.

As seen in Fig. 3a, the (5%Pd + 2.5%Cu)/ACF catalyst metal nanoparticles have a quite broad size distribution with an average diameter of ~7.7 nm. EDX analysis revealed that the larger particles are composed of both Pd and Cu. The smaller particles seem to be only Pd. It can be explained by the fact that palladium deposited on the first step of the material synthesis by adsorption of the precursor followed by its reduction is homogeneously distributed in the form of <2 nm nanoparticles through the ACF microporous network. On the second step of the synthesis, because of the diffusion limitations, copper is catalytically deposited rather on easily accessible Pd nanoparticles placed on the outer activated carbon fiber surface than on Pd nanoparticles seated within the ACF micropores.

Bimetallic nanoparticles in the (2%Pd + 1%Sn)/ACF are smaller ($d \sim 2.3$ nm) than in the previous Pd–Cu sample. They have a quite narrow size distribution (Fig. 3b). EDX analysis revealed that both Pd and Sn are homogeneously distributed over the ACF support. All particles are composed of both Pd and Sn. It is worth to remind that tin was deposited on the second step of the synthesis through the precursor impregnation followed by H_2 reduction and hence it was able to penetrate into the ACF microporous network and to reach all Pd nanoparticles.

Table 1
Some characteristics of the structured catalysts.

Catalyst	SSA_{BET} (m^2/g)	SSA_{BET} (m^2/g_{CNF})	Pore size (nm)	Pore volume (cm^3/g_{carbon})	Metal particle size (nm)
ACF	950	–	<2 (micro-)	0.58	–
(5%Pd + 2.5%Cu)/ACF	663	–	<2	0.6	7.7
(1%Pd + 0.5%Cu)/ACF	780	–	<2		
(5%Pd + 2.5%Sn)/ACF	780	–	<2		
(2%Pd + 1%Sn)/ACF	740	–	<2		2.3
(1%Pd + 0.5%Sn)/ACF	780	–	<2		
(0.3%Pd + 0.15%Sn)/ACF	750	–	<2		
5%CNF/SMF	13.1	263	20/85 (meso-)	0.62	–
(0.3%Pd + 0.15%Cu)/5%CNF/SMF	12.5	250	20/85		2.0
(0.3%Pd + 0.15%Sn)/5%CNF/SMF	14	280	20/85		2.0/7.0

Fig. 4a shows the images of the (0.3%Pd + 0.15%Cu)/5%CNF/SMF. The sample is highly homogeneous. Monodispersed metal nanoparticles ($d \sim 2.0$ nm) are uniformly distributed over the CNF surface. EDX analysis confirmed that nanoparticles are composed of both Pd and Cu. The uniform contrast inside each nanoparticle seems to exclude that the metals are segregated. They form a bimetallic mixture with homogeneous distribution of the two metals.

The (0.3%Pd + 0.15%Sn)/5%CNF/SMF catalyst is also very homogeneous with metal nanoparticles densely dispersed on the CNF surface (Fig. 4b). In this case nanoparticles have bimodal size distribution with peaks at 2.0 and 7.0 nm. EDX analysis revealed that the larger particles are composed of both Pd and Sn. At the same time, it is clearly seen from the high magnification image that the most of nanoparticles have a core–shell structure [36]. It can be deduced that the core consists of Pd whereas the shell (~2 nm thickness) consists of Sn. The smaller particles have the same contrast than the shell regions and could be ascribed to pure Sn.

3.3. Catalytic performance of bi-metallic structured carbon-based catalysts in nitrate reduction

3.3.1. Semi-batch mode

The activity and selectivity of the catalysts based on different structured supports were first measured in a semi-batch mode. Fig. 5 represents a time dependence of the nitrate conversion and N_2 selectivity for the Pd–Cu and Pd–Sn ACF-based catalysts. The results indicate that NO_3^- hydrogenation is a consecutive reaction going through NO_2^- as an intermediate. After the formation, NO_2^- -ions are reduced to either N_2 or NH_4^+:

$$NO_3^- \xrightarrow[k_1]{H_2} NO_2^- \xrightarrow[k_2]{H_2} [N^*] \begin{cases} \nearrow N_2 \\ \searrow NH_4^+ \end{cases}$$

The detected concentration of intermediate NO_2^- -ions is much higher in the case of the (2.5%Cu + 5%Pd)/ACF than for the (2.5%Sn + 5%Pd)/ACF (Fig. 5). This indicates that the k_2/k_1 ratio is much greater for the Sn-modified catalysts as compared to the Cu-modified catalysts.

NO_2^- hydrogenation on the second step is critical for the reaction selectivity. It is known that pure Pd is inactive in nitrate hydrogenation. That is why bimetallic catalysts are needed to carry out the reaction [1]. At the same time, nitrite hydrogenation can take place on both Pd and bimetallic catalysts. Thus, the reaction selectivity is dependent on the chemical composition of a bimetallic active phase, the presence of Pd^0 as well as on the reaction conditions.

The (5%Pd + 2.5%Sn)/ACF catalyst was found to be more active and selective towards N_2 than the (5%Pd + 2.5%Cu)/ACF (Fig. 5). As it was shown by STEM, palladium and tin are perfectly mixed and form small Pd–Sn nanoparticles ($d \sim 2.3$ nm) homogeneously distributed over ACF (Fig. 3b). We can conclude that tin effectively modifies Pd^0 resulting in an improved catalyst performance. In the (5%Pd + 2.5%Cu)/ACF catalyst only a part of Pd^0 nanoparticles, which

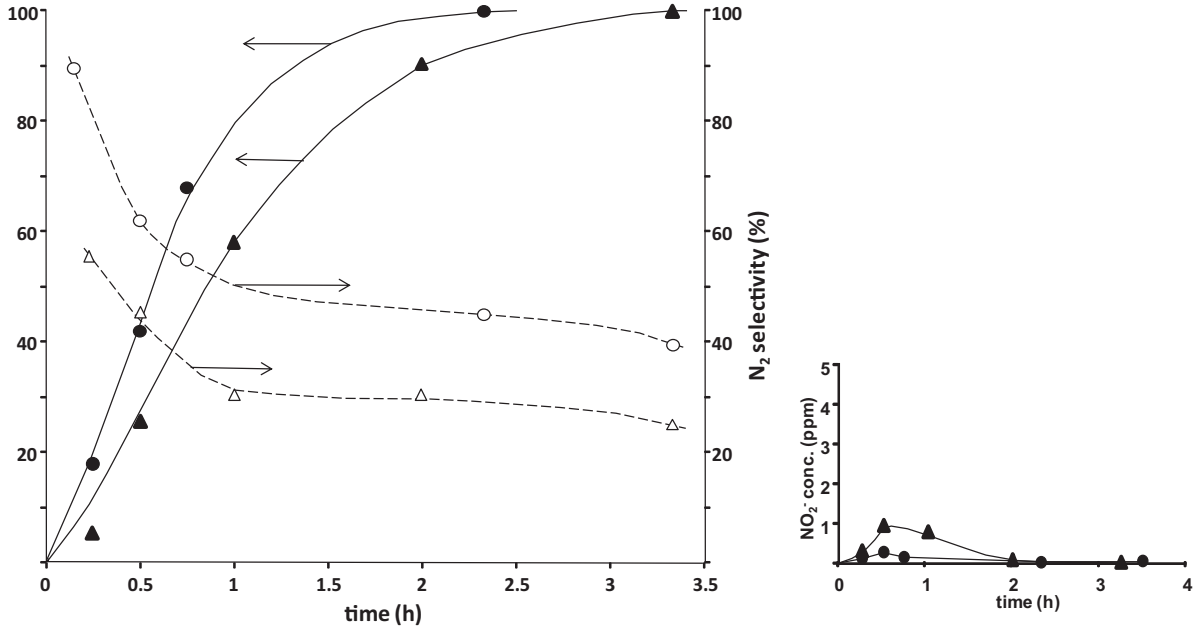

Fig. 5. Nitrate reduction on the (5%Pd + 2.5%Cu)/ACF (▲; △) and (5%Pd + 2.5%Sn)/ACF (●; ○) in a semi-batch mode ($C^0_{NO_3^-} = 100$ mg/l; $m_{cat} = 0.8$ g/l; $T = 25$ °C; pH 6.5).

Table 2
The catalyst performance in a continuous mode with natural water.

Catalyst	NO_3^- conversion (%)	Activity $mol_{NO_3^-}/mol_{Pd} \cdot S$)	N_2 selectivity (mol%)	NH_4^+ selectivity (mol%)	NO_2^- selectivity (mol%)
(5%Pd + 2.5%Cu)/ACF	60	1.4×10^{-4}	39	54	7
(1%Pd + 0.5%Cu)/ACF	70	12×10^{-4}	30.3	69	0.7
(5%Pd + 2.5%Sn)/ACF	90	1.74×10^{-4}	60	39.9	0.1
(2%Pd + 1.0%Sn)/ACF	70	4.1×10^{-4}	60	39.94	0.06
(1%Pd + 0.5%Sn)/ACF	70	5.2×10^{-4}	70	29.5	0.5
(0.3%Pd + 0.15%Cu)/5%CNF/SMF	25	9.8×10^{-4}	56	39	5
(0.3%Pd + 0.15%Sn)/5%CNF/SMF	25	11×10^{-4}	75	22	3

is accessible for the Cu precursor during the synthesis, is modified by copper (Fig. 3a). The co-existence of relatively big Pd–Cu nanoparticles ($d \sim 7.7$ nm) and small Pd^0 nanoparticles could be a reason for the lower activity and selectivity in this case, since pure Pd^0 nanoparticles are less N_2 selective in intermediate NO_2^- reduction as compared to Pd–Cu ones [12,25].

In both cases a drop of the N_2 selectivity was observed at higher conversions indicating the presence of mass-transfer limitations in ACF micropores. It is known that the denitrification reaction rate and selectivity decrease with the local pH. OH^- -anions produced during the catalytic nitrate reduction ($2NO_3^- + 5H_2 \rightarrow N_2 + 2OH^- + 4H_2O$) concentrate inside micropores and block active sites on the nanoparticle surface influencing on the reaction pathway [5].

Unlike the microporous ACF-based catalyst, OH^- -anions seem to be easily removed from the CNF mesopore network into the bulk liquid phase without affecting the reaction selectivity. In order to check the influence of the support porosity on the catalyst selectivity, a catalyst with a low-concentrated (Pd–Sn) active phase supported on mesoporous CNF/SMF was tested in a semi-batch mode. As can be seen from Fig. 6, the (0.3%Pd + 0.15%Sn)/5%CNF/SMF catalyst is really selective towards N_2 in a wide range of conversion confirming the advantage of mesoporous CNF-based catalysts in the liquid phase reduction.

3.3.2. Continuous mode

Table 2 shows the catalytic activity (measured after 6 h and calculated per gram of Pd) and selectivity for nitrate reduction (with natural water) over the structured bimetallic carbon-based catalysts tested in a plug-flow reactor. The time course of nitrate hydrogenation over two selected Sn-modified catalysts is presented in Fig. 7. Long-term experiments were carried out to test the catalyst stability. The catalysts were found to be stable during 30 h on stream.

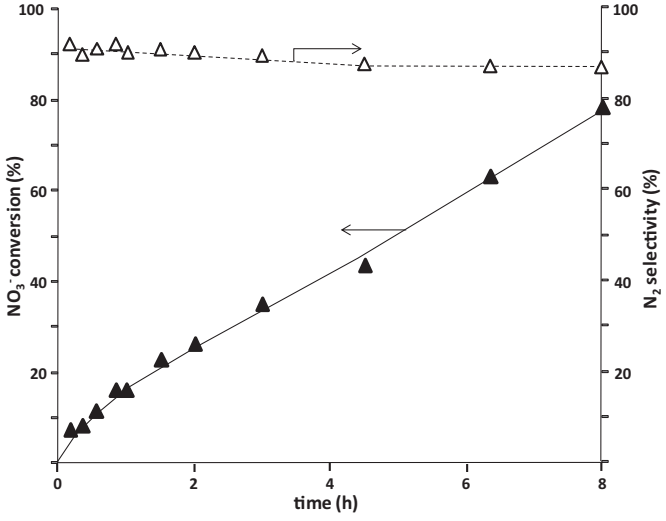

Fig. 6. Nitrate reduction on the (0.3%Pd + 0.15%Sn)/5%CNF/SMF in a semi-batch mode ($C^0_{NO_3^-} = 100$ mg/l; $m_{cat} = 0.8$ g/l; $T = 25$ °C; pH 6.5). Maximum $C_{NO_2^-}$ during the reaction was <0.2%.

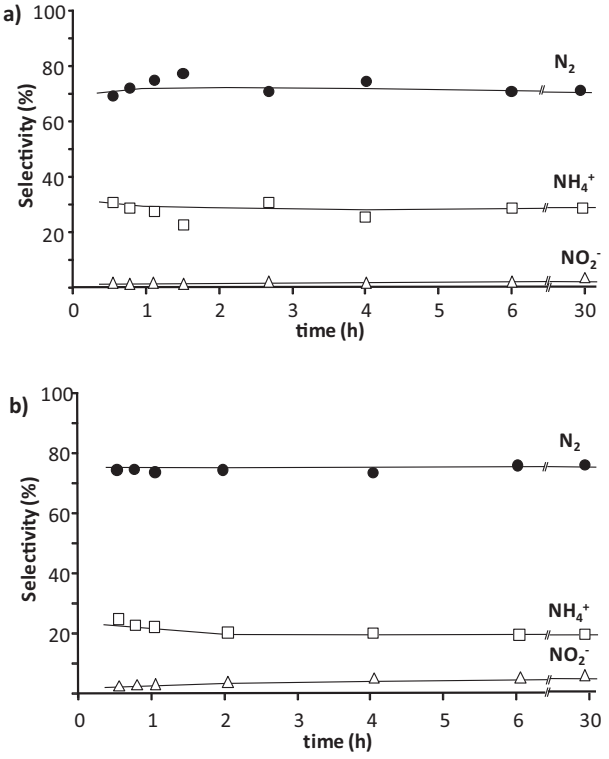

Fig. 7. Nitrate reduction (natural water) on (a) (1%Pd + 0.5%Sn)/ACF at $X_{NO_3^-} = 70\%$ and (b) (0.3%Pd + 0.15%Sn)/5%CNF/SMF at $X_{NO_3^-} = 25\%$ in a continuous mode (natural water, $C^0_{NO_3^-} = 100$ mg/l; $m_{cat} = 1$–3 g; $F_{liquid} = 5$ ml/min; $T = 25$ °C; pH 6.5).

Table 2 demonstrates that all Pd–Sn catalysts are more selective towards N_2 as compared to the Pd–Cu analogs. The specific activity of the ACF-based catalysts increases with a decrease of the metal loading. At higher loadings, nanoparticles situated within narrow ACF micropores seem to be partly inaccessible. The highest activity obtained on the low-concentration ACF-based catalysts is close to the activity of the mesoporous CNF/SMF-based catalysts, while selectivity to N_2 is about double in the latter.

Two catalysts supported on CNF/SMF exhibit similar activities, despite the fact that Pd–Cu catalyst has smaller particle size than Pd–Sn. It can be attributed to the specific Pd–Sn interaction governed by the nature of the second metal.

4. Conclusions

Bimetallic (Pd–Cu, Pd–Sn) nanoparticles were supported on structured ACF and CNF/SMF, characterized and tested in nitrate reduction using synthetic and natural polluted waters. The tests were carried out in both semi-batch and continuous modes.

According to the obtained results, the following conclusions can be drawn:

1. Structured fibrous catalysts are suitable for natural water denitrification due to the arrangement of the catalytic bed with a low pressure drop, even flow distribution and reduced mass transport limitations. The mesoporous CNF/SMF support allows avoiding internal diffusion limitations.
2. Catalytically active (Pd–Cu) nanoparticles (Pd:Cu = 2:1) are composed of bimetallic mixture with a homogeneous metal distribution, whereas (Pd–Sn) nanoparticles (Pd:Sn = 2:1) have a core–shell structure. The nanoparticles structure and the nature of the second metal are responsible for the observed difference in catalytic behavior, namely, for the higher N_2-selectivity of supported (Pd–Sn) nanoparticles.
3. The mesoporous (0.3%Pd + 0.15%Sn)/5%CNF/SMF demonstrates the best activity and N_2 selectivity (~75%) in an open flow reactor. To the best of our knowledge, this is the highest result obtained for the nitrate reduction in polluted natural water from an aquifer in a continuous mode.

Acknowledgments

This work was carried out with the financial support of the European Community's Seventh Framework Programme (FP7/2007–2013) under grant agreement no. 226347.

References

[1] K.D. Vorlop, T. Tacke, Chemie Ingenieur Technik 61 (1989) 836–837.
[2] S. Hörold, K.D. Vorlop, T. Tacke, M. Sell, Catalysis Today 17 (1993) 21–30.
[3] K.D. Vorlop, U. Prüsse, Environmental Catalysis in: F.K.J.G. Janssen, R.A. van Santen (Eds.), Catalytic Science Series, vol. 1, Imperial College Press, London, 1999, p. p195.
[4] J. Batista, A. Pintar, M. Ceh, Catalysis Letters 43 (1997) 79–84.
[5] A. Pintar, M. Setinc, J. Levec, Journal of Catalysis 174 (1998) 72–87.
[6] A. Pintar, G. Bercic, J. Pintar, AIChE Journal 44 (1998) 2280–2292.
[7] U. Prüsse, K.D. Vorlop, Journal of Molecular Catalysis A: Chemical 173 (2001) 313–328.
[8] S.M. Jung, E. Godard, S.Y. Jung, K.C. Park, J.U. Choi, Catalysis Today 87 (2003) 171–177.
[9] A. Pintar, J. Batista, I. Musevic, Applied Catalysis B: Environmental 52 (2004) 49–60.
[10] A.E. Palomares, J.G. Prato, A. Corma, Journal of Catalysis 221 (2004) 62–66.
[11] A. Garron, K. Lázár, F. Epron, Applied Catalysis B: Environmental 59 (2005) 57–69.
[12] J. Sá, H. Vinek, Applied Catalysis B: Environmental 57 (2005) 247–256.
[13] J. Sá, D. Gasparovicova, K. Hayek, E. Halwax, J.A. Anderson, H. Vinec, Catalysis Letters 105 (2005) 209–217.
[14] A. Garron, K. Lázár, F. Epron, Applied Catalysis B: Environmental 65 (2006) 240–248.
[15] A. Devadas, S. Vasudevan, F. Epron, Journal of Hazardous Materials 185 (2011) 1412–1417.
[16] M. D'Arino, F. Pinna, G. Strukul, Applied Catalysis B: Environmental 53 (2004) 161–168.
[17] A. Garron, F. Epron, Water Research 29 (2005) 3073–3081.
[18] N. Barrabés, A. Dafinov, F. Medina, J.E. Sueiras, Catalysis Today 149 (2010) 341–351.
[19] A.E. Palomares, C. Franch, A. Corma, Catalysis Today 172 (2011) 90–94.
[20] A. Cybulski, J.A. Moulijn, Catalysis Review Science Engineering 36 (1994) 179–270.
[21] E. Garcia-Bordeje, I. Kvande, D. Chen, M. Ronning, Advanced Materials 18 (2006) 1589–1592.
[22] V. Höller, K. Rådevik, I. Yuranov, L. Kiwi-Minsker, A. Renken, Applied Catalysis B: Environmental 32 (2001) 143–150.
[23] Y. Matatov-Meytal, V. Barelko, I. Yuranov, M. Sheintuch, Applied Catalysis B: Environmental 27 (2000) 127–135.
[24] N. Semagina, M. Grasemann, N. Xanthopoulos, A. Renken, L. Kiwi-Minsker, Journal of Catalysis 251 (2007) 213–222.
[25] Y. Yoshinaga, T. Akita, I. Mikami, T. Okuhara, Journal of Catalysis 207 (2002) 37–45.
[26] L. Lemaignen, C. Tong, V. Begon, R. Burch, D. Chadwick, Catalysis Today 75 (2002) 43–48.
[27] Y. Sakamoto, M. Kanno, T. Okuhara, Y. Kamiya, Catalysis Letters 125 (2008) 392–395.
[28] O.S.G.P. Soares, J.J.M. Órfão, M.F.R. Pereira, Applied Catalysis B: Environmental 91 (2009) 441–448.
[29] Y. Matatov-Meytal, M. Sheintuch, Catalysis Today 102 (2005) 121–127.
[30] P. Serp, M. Corrias, P. Kalek, Applied Catalysis A-General 253 (2003) 337–358.
[31] P. Tribolet, L. Kiwi-Minsker, Catalysis Today 102 (2005) 15–22.
[32] P. Tribolet, L. Kiwi-Minsker, Catalysis Today 105 (2005) 337–343.
[33] B. Louis, D. Bégin, M.J. Ledoux, C. Pham-Huu, Ordered Porous Solids, 2009 23 (2009) 621–649.
[34] D. Bulushev, I. Yuranov, E. Suvorova, F. Buffat, L. Kiwi-Minsker, Journal of Catalysis 224 (2004) 8–17.
[35] U. Matatov-Meytal, M. Sheintuch, Catalysis Communications 10 (2009) 1137–1141.
[36] D. Häussler, F. Liu, W. Jäger, W. Rechberger, F. Hofer, X.B. Zhang, Microscopy and Microanalysis 13 (2007) 434–435.